Tropopause Evolution in a Rapidly Intensifying Tropical Cyclone: A Static Stability Budget Analysis

Patrick Duran* and John Molinari

University at Albany, State University of New York, Albany, NY

Corresponding author address: Department of Atmospheric and Environmental Sciences, University at Albany, State University of New York, 1400 Washington Avenue, Albany, NY.

E-mail: pduran2008@gmail.com

ABSTRACT

We have some cool results!

1. Introduction

There will be a whole bunch of papers cited here...

2. Model Setup

Put description of Fig. 1 in this section.

Don't forget to mention 1-2-1 smoother.

3. Budget Computation

Add details of budget computation here...

4. Results

a. Static stability evolution

The average N^2 over the first day of the simulation (Fig. 2a) indicates the presence of a static stability maximum about 400 m above the cold-point tropopause. This lower-stratospheric stable layer had begun to erode during the initial spin-up period, with the maximum destabilitzation occurring at the innermost radii. This decrease in static stability continued into the second day of the simulation (Fig. 2b) as the storm intensified to hurricane strength (Fig. 1). Destabilization was particularly pronounced over the developing eye, where the time-mean cold-point tropopause height increased by up to 400 m compared to the previous day. Over the developing eyewall and outer rainband regions, meanwhile, the tropopause height remained nearly constant. During the third day of the simulation (Fig. 2c), static stability over the eye continued to decrease, and the cold-point tropopause height rose to 18.3 km at the storm center. The tropopause sloped sharply downward over the innermost radii, reaching the 16.4-km level near the 50-km radius. This local minimum in tropopause height corresponded to the eyewall region, where upper-tropospheric

static stability increased during this time period. Outside of the eyewall region, static stability began to increase in the layer immediately overlying the cold-point tropopause. This stable layer sloped upward with radius, which corresponded to an upward-sloping tropopause radially outside of the eywall region. Over the next 24 hours (Fig. 2d), as the storm's maximum 10-m wind speed leveled off near 80 m s^{-1} (Fig. 1), the upper-tropospheric static stability within the eyewall region continued to strengthen, as did the static stability just above the cold-point tropopause radially outside of the eyewall. As the stable layer strengthened, its altitude rose slightly, which corresponded to a slight increase in tropopause height outside of the eyewall during this period. Within the upper troposphere radially outside of the eyewall, meanwhile, static stability decreased such that it was nearly neutral in a thin layer between the 120- and 150-km radii. The eye region likewise continued to destabilize, and the cold-point tropopause height increased to a level above 18.5 km. This static stability evolution closely follows that observed in Hurricane Patricia (2015; Duran and Molinari 2018).

b. Static stability budget analysis

The left column of Fig. 3 depicts 24-hour changes in N^2 over each of the four days of the simulation. These represent bulk changes computed by subtracting the instantaneous N^2 at the initial time from the instantaneous N^2 at the final time. The middle column of Fig. 3 represents the change in N^2 computed using Eq. XXX and the method described in Section 3. The residual between these two computations (Fig. 3, right column) is much smaller than the change in N^2, meaning that the budget peforms well within the analysis domain.

To determine which of the budget terms are most important, a time series of the contribution of each of the budget terms in Eq. XXX to the tropopause-layer static stability tendency is plotted in Fig. 4. For this figure, each of the budget terms is computed using the method described in

Section 3, except with 1-hour averaging intervals instead of 24-hour intervals. The absolute values of these tendencies are then averaged over the radius-height domain depicted in Fig. 3 and plotted as a time series[1]. Advection (Fig. 4, red line) plays an important role in the mean tropopause-layer static stability tendency at all times, and vertical turbulence (Fig. 4, blue line) and radiation (Fig. 4, dark green line) both become important after 48 hours. Although the contribution from horizontal turbulence (Fig. 4, purple line) becomes more important after 72 hours, it is confined to a very small region immediately surrounding the eyewall tangential velocity maximum (not shown), and is negligible throughout the rest of the tropopause layer. The remaining two processes - microphysics and dissipative heating (Fig. 4, orange and light green lines, respectively) - lie atop one another near zero. These time series indicate that, at all times, three budget terms dominate the tropopause-layer static stability tendency: advection, vertical turbulence, and radiation. Variations in the magnitude and spatial structure of these terms drive the static stability changes depicted in Fig. 2; subsequent sections will focus on these variations and what causes them.

(i) 0-24 hours The first 24 hours of the simulation was characterized by a weakening of the lower-stratospheric static stability maximum above 17 km (Fig. **??**a, purple shading) and an increase in static stability below (green shading). Although these tendencies extended out to the 200-km radius, they were particularly pronounced at innermost radii. A comparison of the contributions of advection (Fig. **??**b), vertical turbulence (Fig. **??**c), and radiation (Fig. **??**d) reveals that advection is primarily responsible for the change in static stability during this period. ...Explain this in the context of radial and vertical velocities...

[1]It will be seeen in subsequent figures that each of the terms contributes both positively and negatively to the N^2 tendency within the analysis domain. Thus, taking an average over the domain tends to wash out the positive and negative contributions. To circumvent this problem, the absolute value of each of the terms is averaged, yielding a time series of the mean magnitude of each budget term.

(ii) 24-48 hours During the second day of the simulation, the lower-stratospheric stable layer continued to weaken (Fig. 6a). This weakening trend in the 16.75-17.75-km layer extended from the 50 km radius outward to past 200 km, and was primarily driven by advection (Fig. 6b). Below this layer, static stability began to increse slightly. This stabilization had contributions from both vertical turbulence (Fig. 6c) and radiation (Fig. 6d) in the 16-16.5-km layer. ...Explain this in context of mean vertical mixing coefficient and mean radiative heating tendency... Meanwhile, radially inward of 60 km, static stability below 17.5 km continued to weaken, primarily due to advective processes.

(iii) 48-72 hours The third day of the simulation marked a dramatic change in the structure of the tropopause-layer static stability tendencies. During this time, static stability increased markedly in an upward-sloping region within the 30-60-km radial band (Fig. 7a), and also increased within the 16.75-17.5-km layer out to at least the 200-km radius. As this layer stabilized, the layer immediately below it destabilized in a broad region extending from 60-200 km. Examination of the contribution from total advection (Fig. 7b) reveals that advection no longer dominates the static stability tendencies. Instead, a combination of vertical turbulence (Fig. 7c) and radiation (Fig. 7d) overcomes the destabilizing influence of advection to create the layer of increasing static stability. Meanwhile, the destabilizing influence of vertical turbulence in a broad region below 17 km combines with a small region of destabilization due to radiation in the 50-120-km radial band combine to destabilize the layer below 16.5 km in the 50-200-km radial band. Comparing the sum of advection and vertical turbulence (Fig. 7e) to the sum of advection, vertical turbulence, and radiation (Fig. 7f) reveals that radiation plays a fundamental role in the re-strengthening of the lower-stratospheric stable layer during this time.

(iv) 72-96 hours

Acknowledgments. Start acknowledgments here.

References

Duran, P., and J. Molinari, 2018: Dramatic inner-core tropopause variability during the rapid intensification of Hurricane Patricia (2015). *Mon. Wea. Rev.*, **XXX (X)**, XXX–XXX.

LIST OF FIGURES

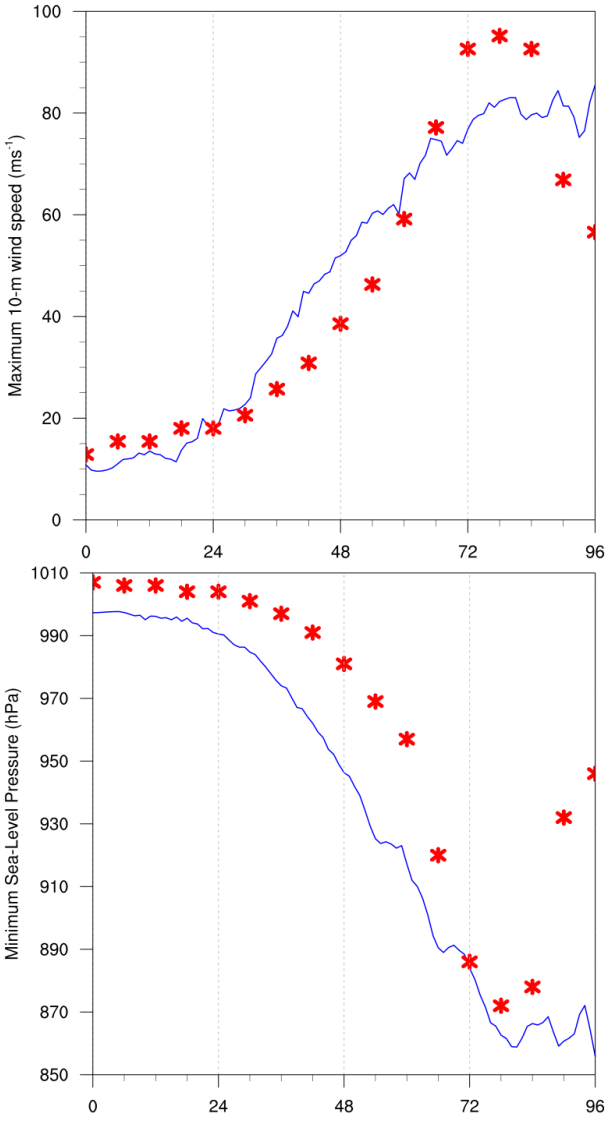

134 FIG. 1. The maximum 10-m wind speed (top panel; m s^{-2}) and minimum sea-level pressure (bottom panel;
135 hPa) in the simulated storm (blue lines) and from Hurricane Patricia's best track (red stars).

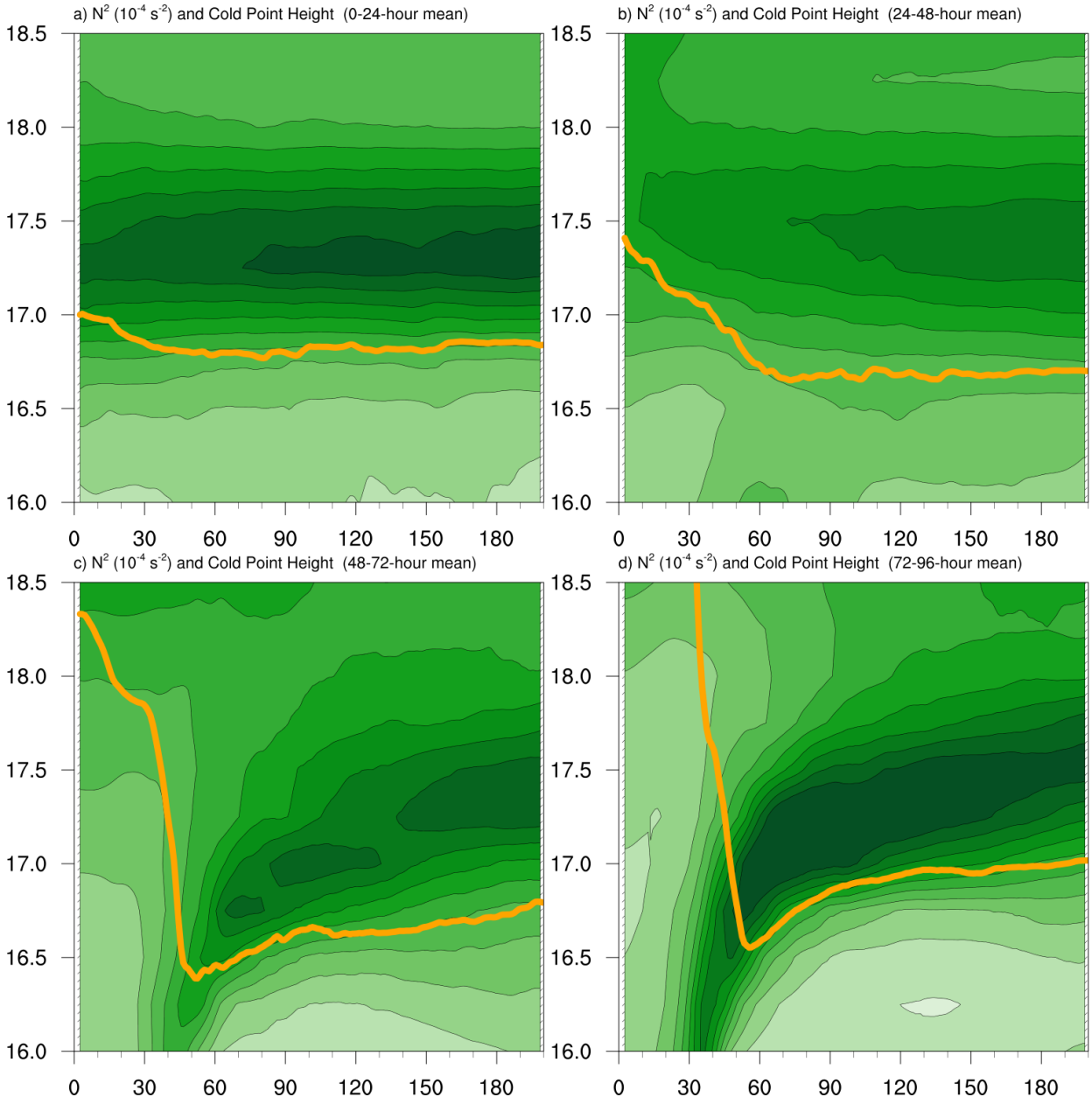

136 FIG. 2. Twenty-four-hour averages of squared Brunt-Väisälä frequency (10^{-4} s^{-2}) over the first four days of
137 the simulation. Orange lines represent the cold-point tropopause computed from the mean temperature field over
138 the same time periods.

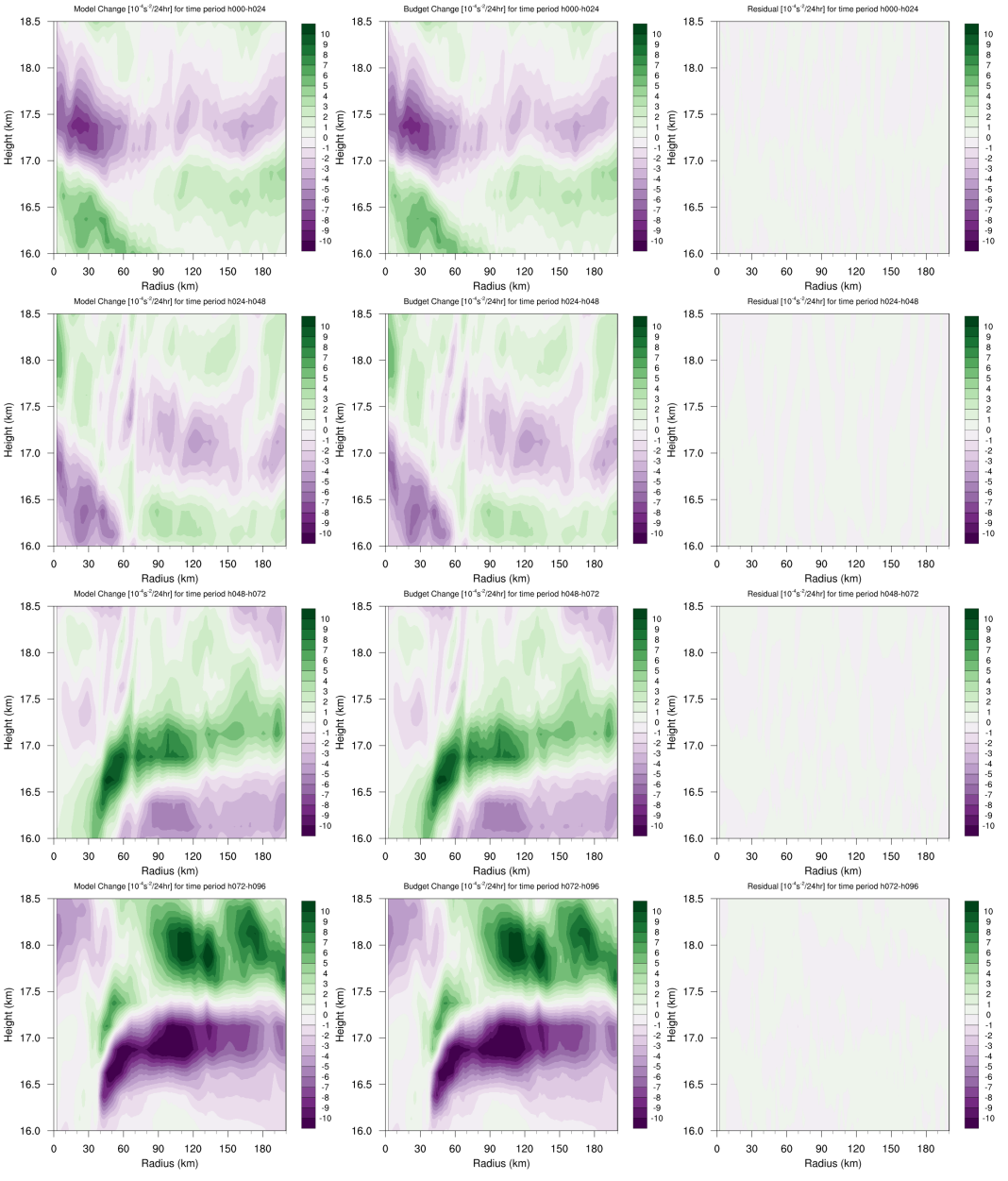

FIG. 3. Left panels: Twenty-four-hour changes in squared Brunt-Väisälä frequency (10^{-4} s^{-2}) over (a) 0-24 hours, (b) 24-48 hours, (c) 48-72 hours, (d) 72-96 hours. Middle Panels: The N^2 change over the same time periods computed using Eq. XXX. Right Panels: The budget residual over the same time periods, computed by subtracting the budget change (middle column) from the model change (left column).

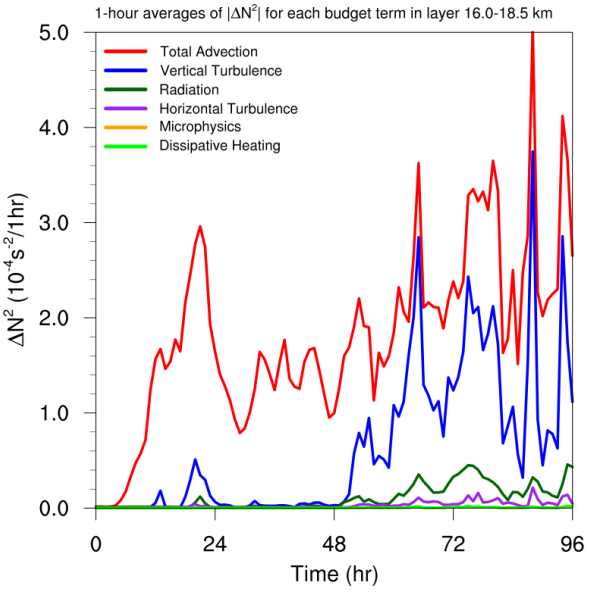

FIG. 4. Time series of the contribution of each of the budget terms to the time tendency of the squared Brunt-Väisälä frequency (N^2; 10^{-4} s^{-2}). For each budget term, the absolute value of the N^2 tendency is averaged both temporally over 1-hour periods (using output every minute), and spatially within the radius-height domain depicted in Fig. 3.

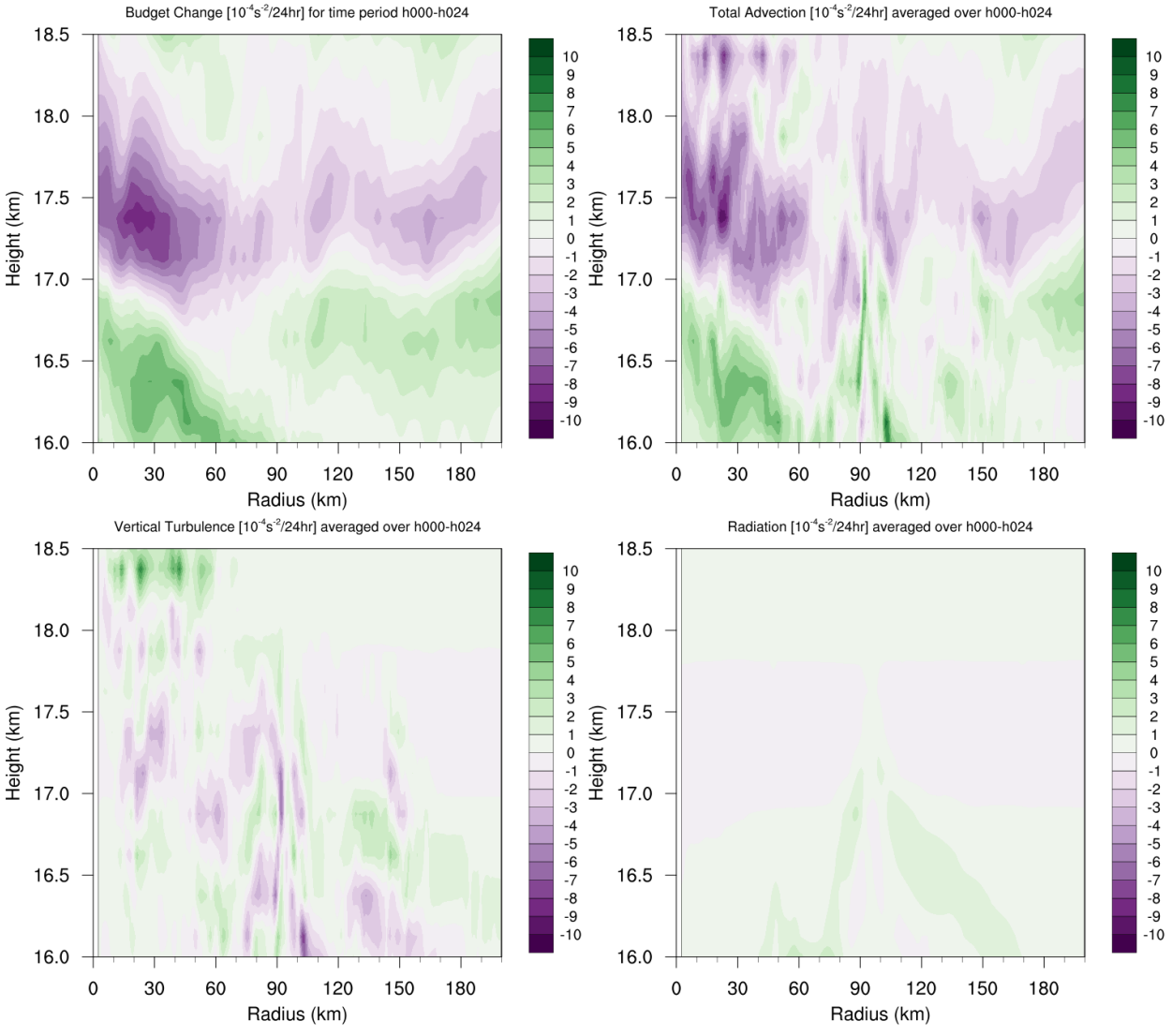

147 FIG. 5. (a) Total change in N^2 over the 0-24-hour period (10^{-4} s^{-2} (24 hr)$^{-1}$) and the contributions to that change
148 from (b) the sum of horizontal and vertical advection, (c) vertical turbulence, and (d) the sum of longwave and
149 shortwave radiation.

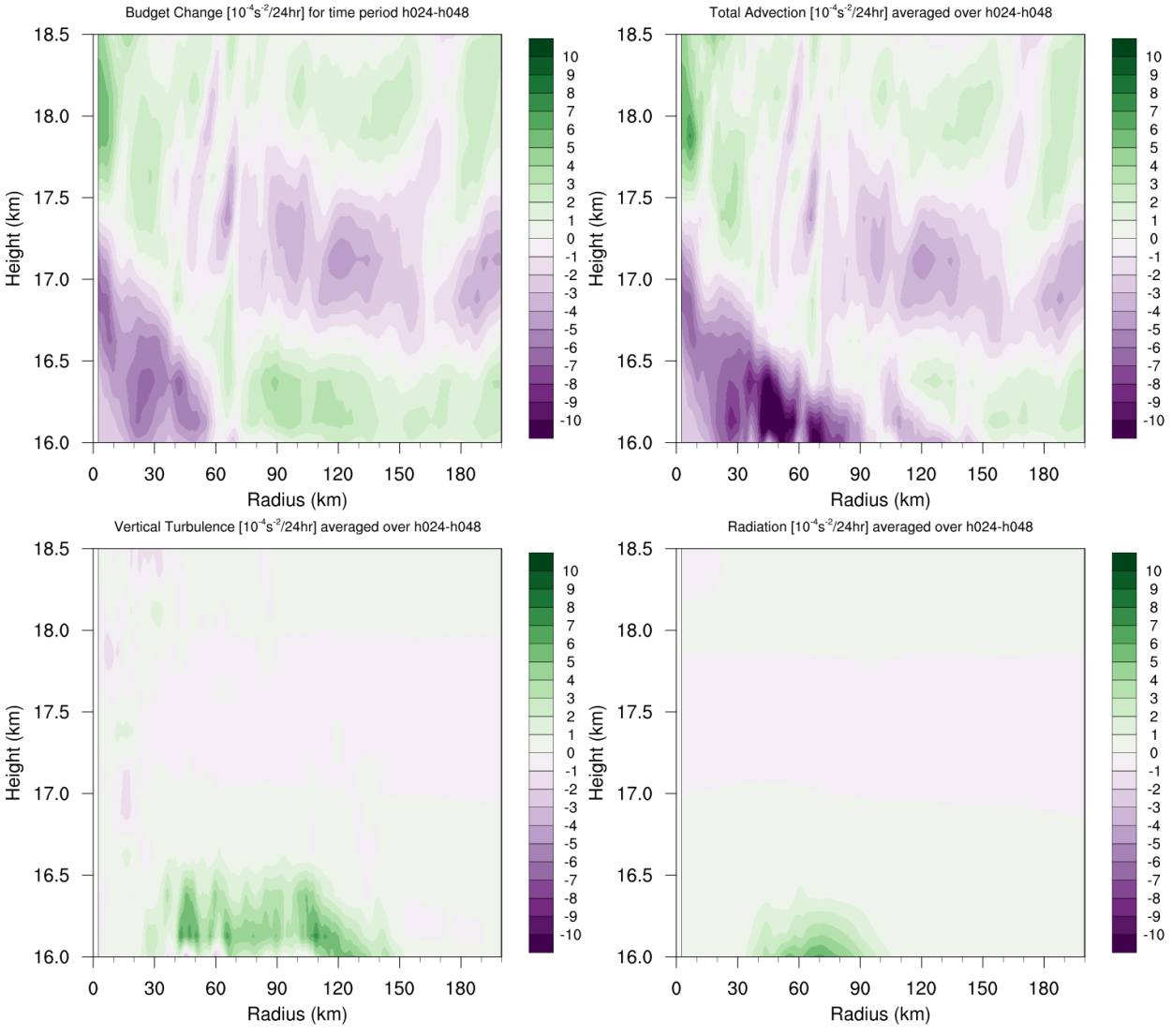

FIG. 6. As in Fig. 5, but for the 24-48-hour period.

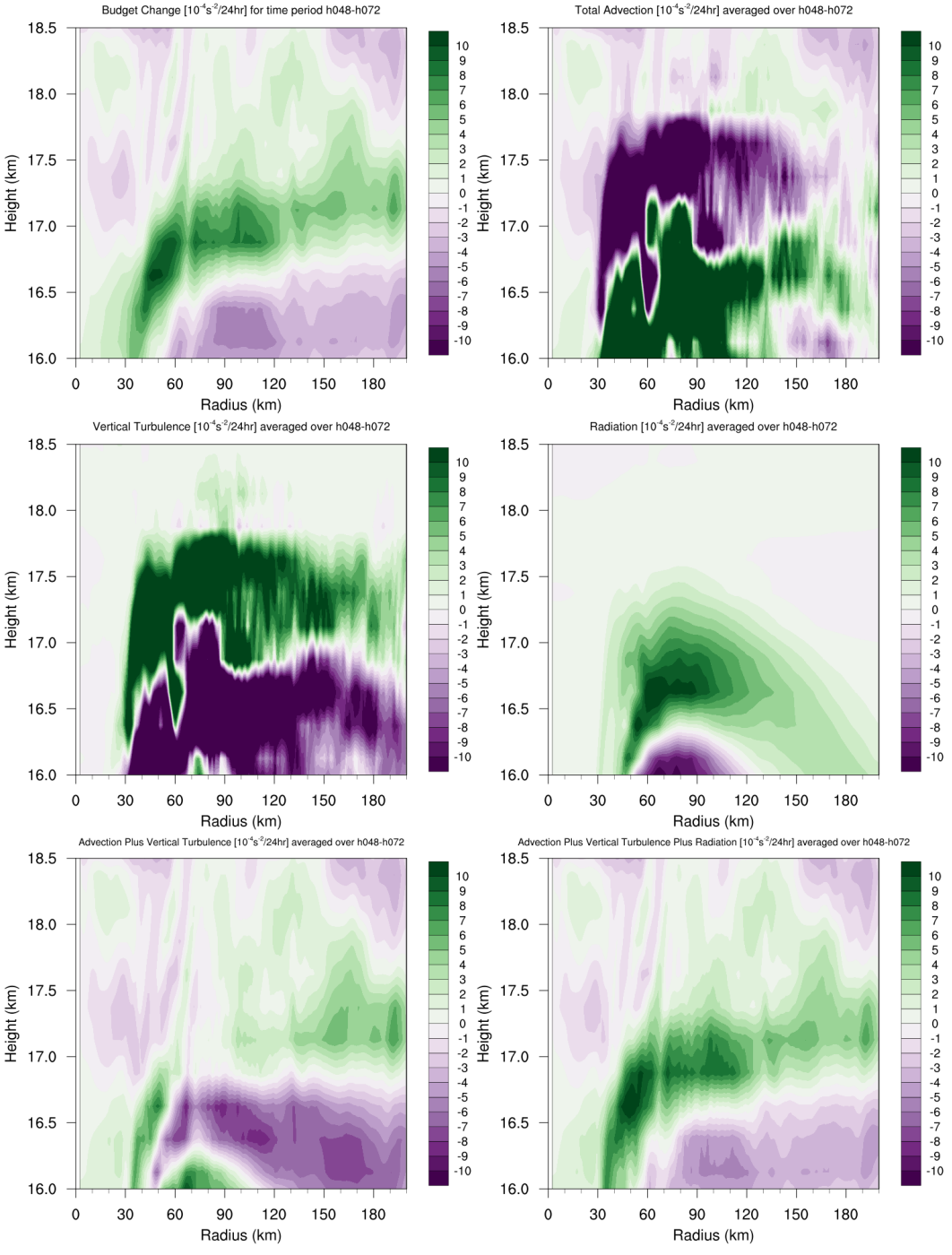

150 FIG. 7. (a) Total change in N^2 over the 48-72-hour period (10^{-4} s^{-2} (24 hr)$^{-1}$) and the contributions to that
151 change from (b) the sum of horizontal and vertical advection, (c) vertical turbulence, (d) the sum of longwave
152 and shortwave radiation, (e) the sum of horizontal advection, vertical advection, and vertical turublence, and (f)
153 the sum of horizontal advection, vertical advection, vertical turbulence, and longwave and shortwave radiation.

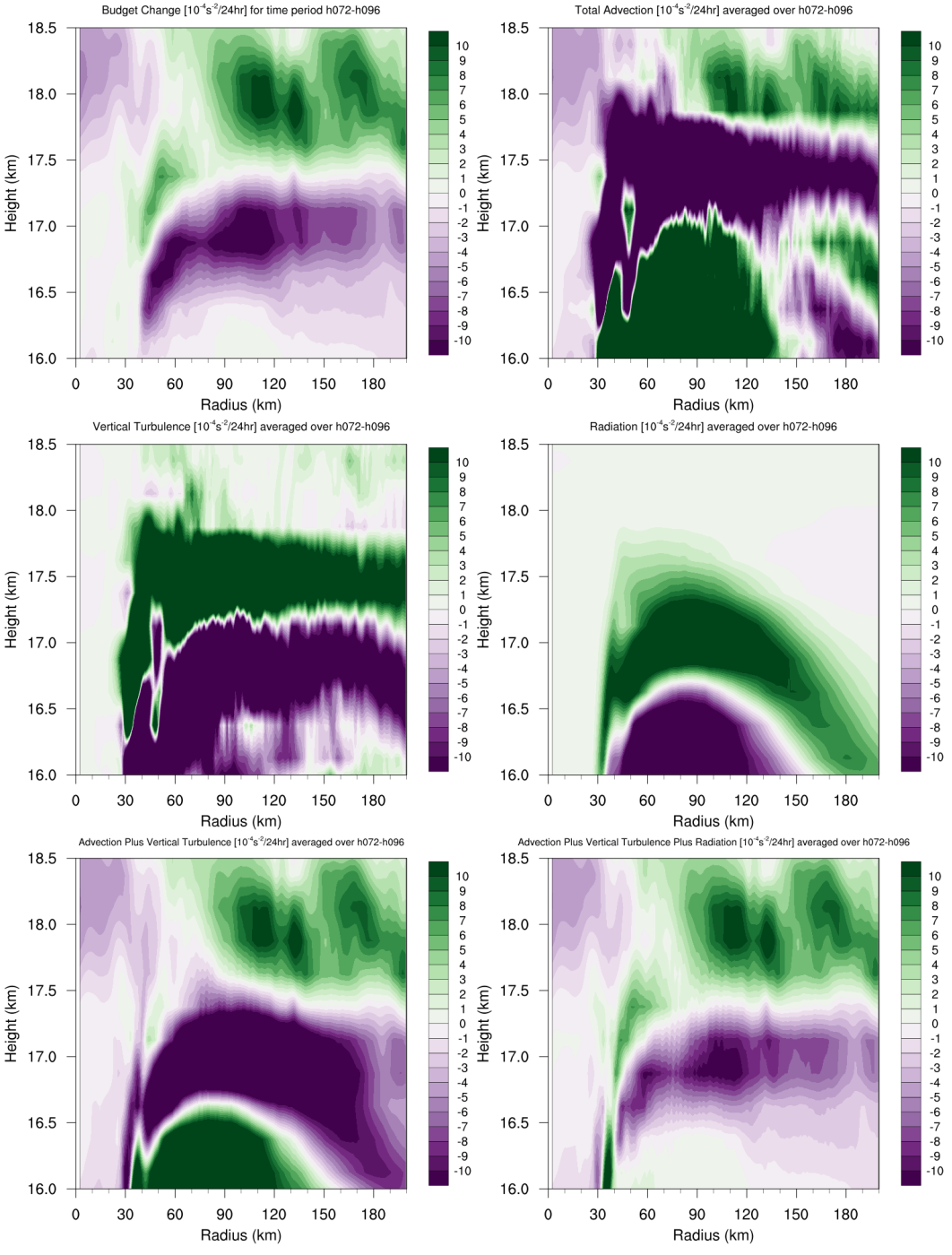

FIG. 8. As in Fig. 7, but for the 72-96-hour period.

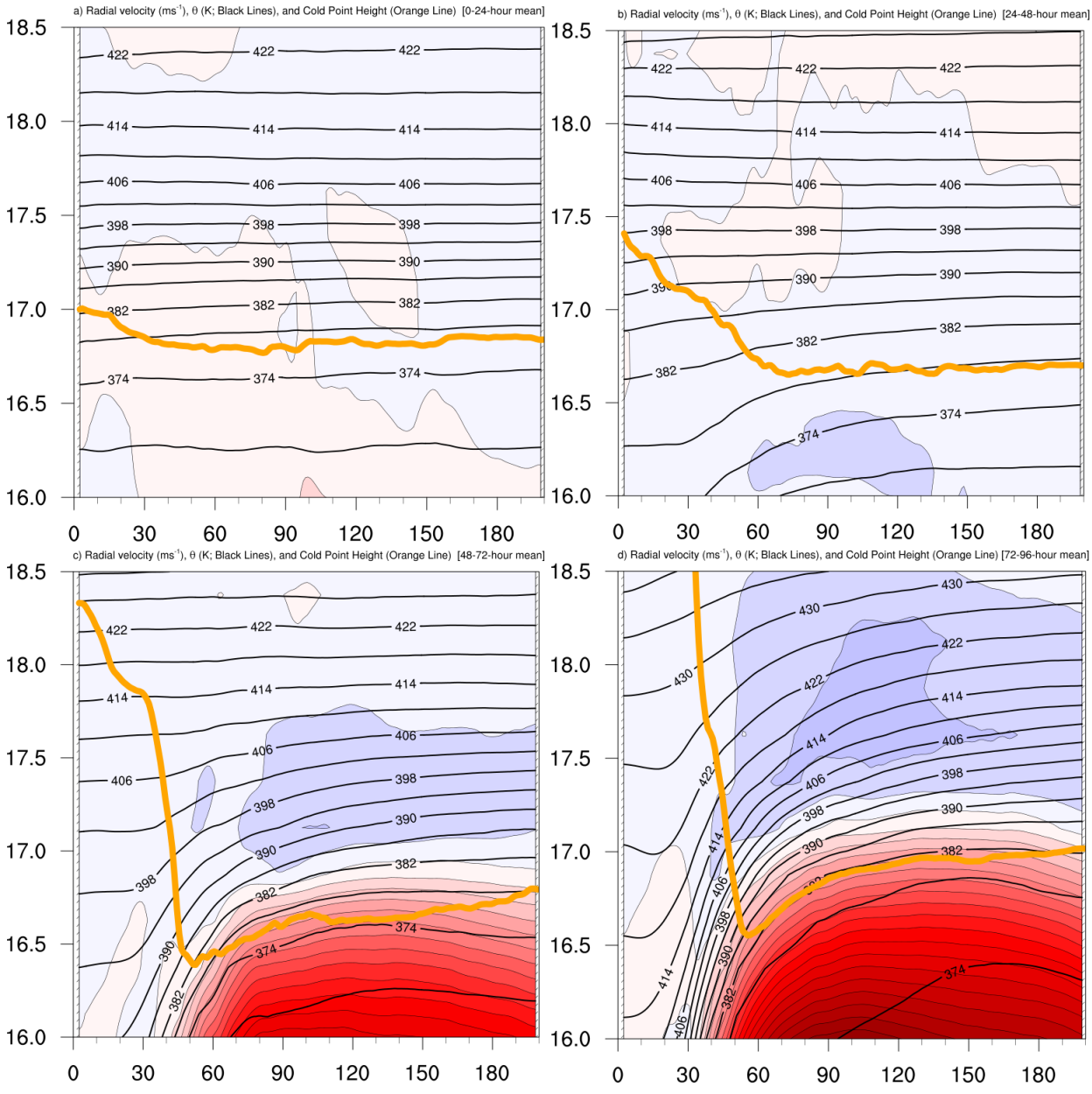

154 FIG. 9. Radial velocity (m s^{-1}; filled contours), potential temperature (K; thick black contours), and cold point
155 tropopause height (orange line) averaged over (a) 0-24 hours, (b) 24-48 hours, (c) 48-72 hours, and (d) 72-96
156 hours.

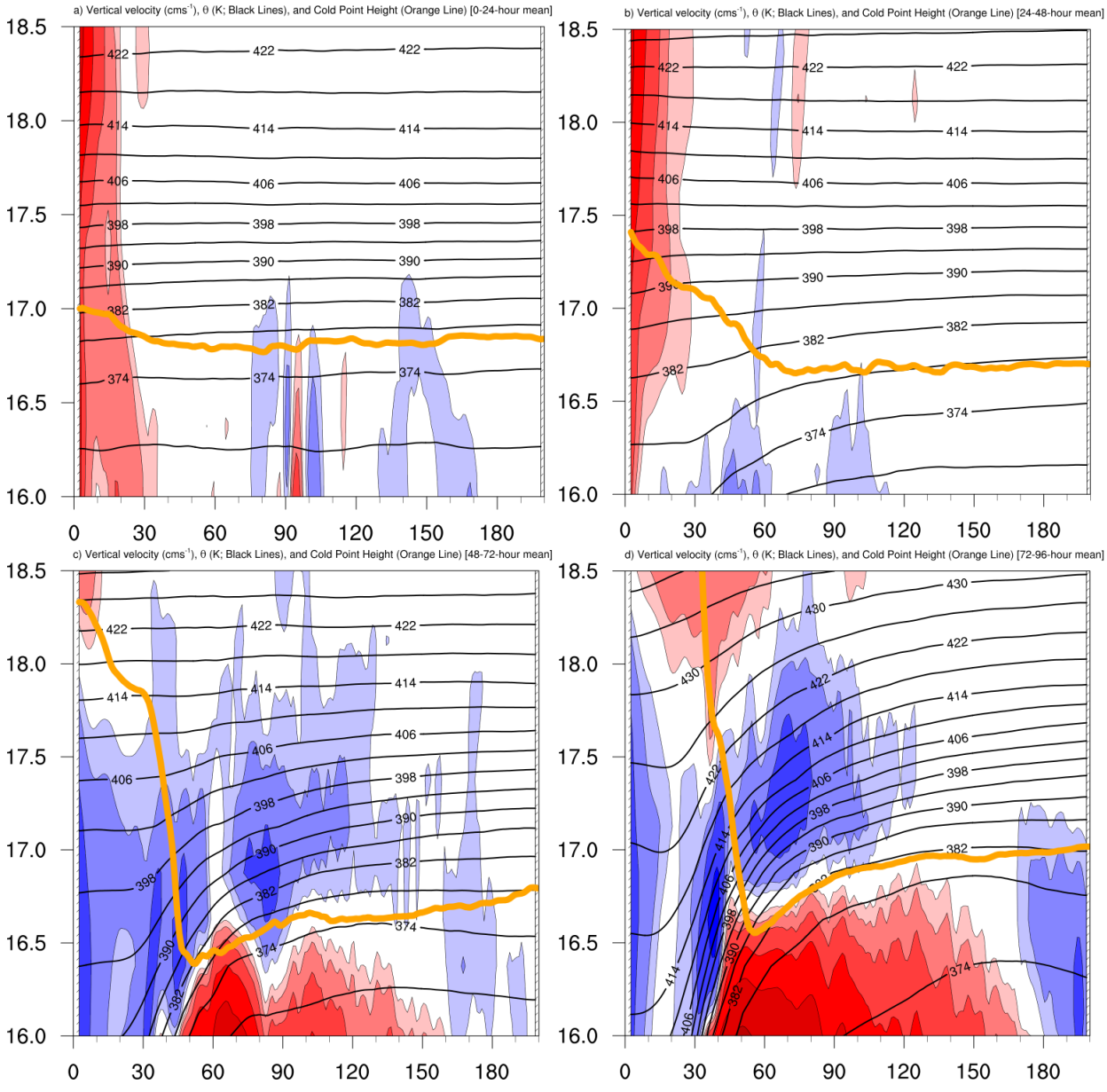

157 FIG. 10. Vertical velocity (cm s^{-1}; filled contours), potential temperature (K; thick black contours), and cold
158 point tropopause height (orange line) averaged over (a) 0-24 hours, (b) 24-48 hours, (c) 48-72 hours, and (d)
159 72-96 hours.

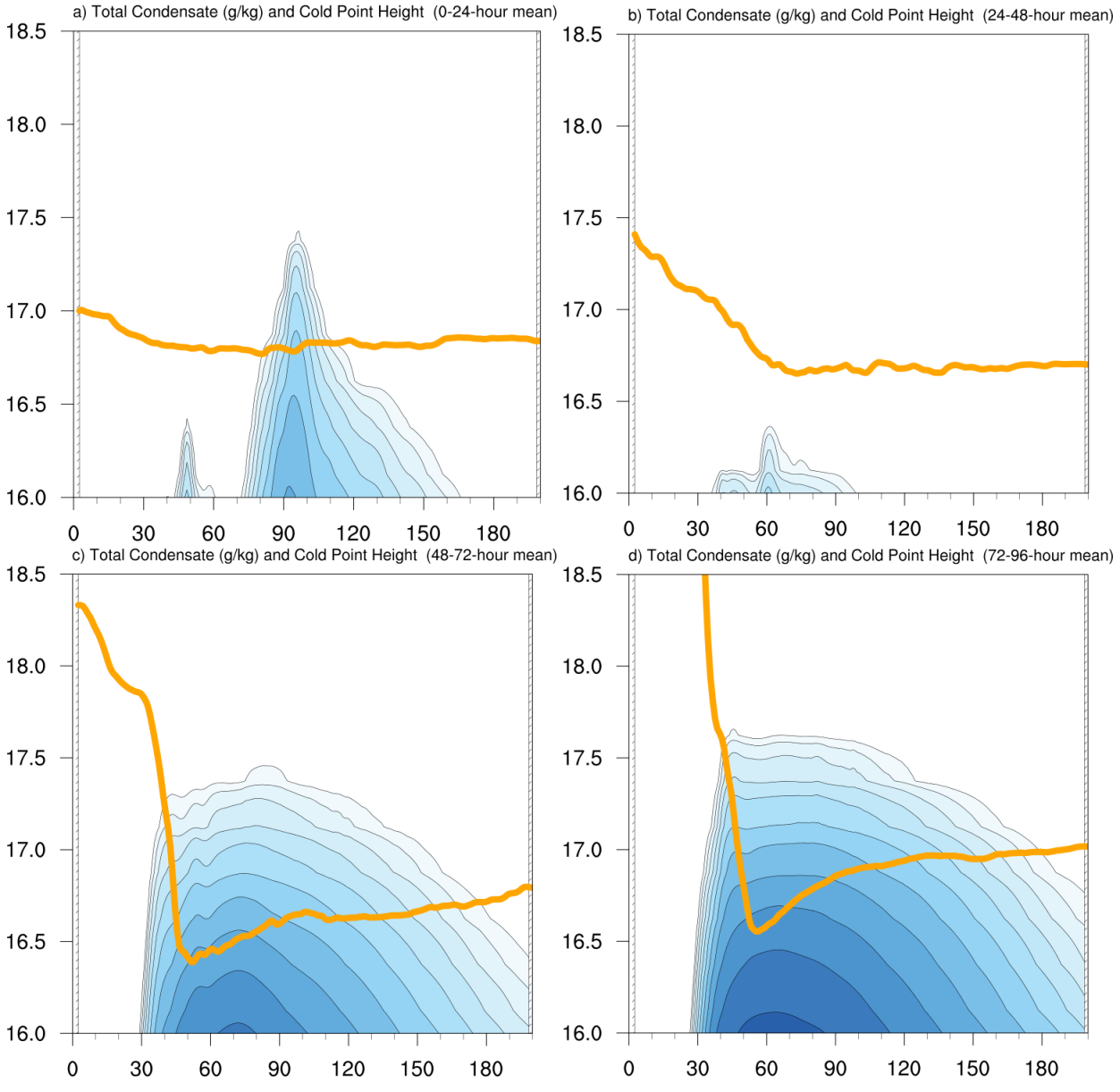

FIG. 11. Total condensate mixing ratio (g kg^{-1}) and cold point tropopause height (orange line) averaged over (a) 0-24 hours, (b) 24-48 hours, (c) 48-72 hours, and (d) 72-96 hours.